High Precision Scanner/Printer Calibrations in Sub-divided Color Spaces

Hiroaki Kotera*, Atsumi Ishige, Hung-Shing Chen, and Ryoichi Saito*

Department of Information and Image Sciences, Chiba University, Chiba, Japan

A variety of color calibration technologies have been developed for input and output devices. Linear or nonlinear matrices have been conveniently applied to correct the color filter's mismatch with color matching function in scanners or suppress the crosstalk by unwanted absorption of colorants in printers. The color matching accuracy is expected to be further improved when the nonlinear matrices are optimized into subdivided smaller color spaces than in single matrix of the entire color space. This article proposes a new method for partitioning the color space into sub-spaces divided by the combinations of luminance, chrominance, radius, or hue angle in CIELAB space so that each sub space includes the constant number of color samples. Linear or nonlinear color correction functions are applied to each subdivided space and the coefficient matrices are optimized individually by the method of least squares. The new method resulted in the high precision color matching with rms color differences ΔE_{ab}*(rms) < 0.5 for flat bed scanner and ΔE_{ab}*(rms) ≈ 2.0 for inkjet printer. The color matching accuracies could approach the colorimetric measurement errors in scanners and mechanical stabilities in printers by the proposed subspace division methods.

Journal of Imaging Science and Technology 43: 178–186 (1999)

Introduction

Color management is a key technology to reproduce the accurate colors across the different media in an electronic color imaging system. The color signals from input devices such as a scanner or camera should be calibrated to match with the correct tristimulus values, and the color masking process is indispensable for printer or copier to eliminate the crosstalk by unwanted absorption in colorants. Linear and nonlinear color correction matrices methods have been conveniently applied to reduce the colorimetric reproduction errors with scanners[3,5,7] or printers.[1,4,6,8] The color reprodution accuracy is expected to be further improved when the color transform matrices or look-up tables in device profiles are optimized in subdivided smaller color spaces rather than in the whole color space.[2,9]

This article discusses the partitioning method of input color space into subspaces, where the equal number of color samples are included in every subspaces to determine the correction matrices.[3] Linear or nonlinear color correction functions are applied to each subspace and the transform matrices are optimized in individual subspace by the method of least squares. The performance of the proposed method is compared with conventional methods.

Color Reproduction System Model

Figure 1 shows the basic color reproduction system model. An input color scanner is modeled as a forward transformer from input tristimulus value T to signal x, while an output printer also works as forward transformer from the drive signal y to tristimulus value T. In the color management system, the scanner signal $x = [R, G, B]^t$ is calibrated to carry the correct tristimulus value $T = [X, Y, Z]^t$ by placing its inverse transformer from x to T behind the input device as follows.

$$T = \Phi_{\mathrm{IN}}{}^{-1}(x) \approx M_{\mathrm{SCAN}} f_S(x) \tag{1}$$

The color corrector is placed in front of the printer to compensate the unwanted absorption of colorants and the nonlinear color mixing characteristics. The color corrector also works as the inverse transformer from the target tristimulus value T to printer drive signal $y = [C, M, Y]^t$ as.

$$y = \Phi_{\mathrm{OUT}}{}^{-1}(T) \approx \mathrm{M}_{\mathrm{PRNT}} f_P(D) \tag{2}$$

Here, the inverse transfiorms $\Phi_{\mathrm{IN}}{}^{-1}(x)$ and $\Phi_{\mathrm{OUT}}{}^{-1}(T)$ are characterized by polynomial expansions $f_S(x)$ and $f_P(D)$ derived from the device input signals.

Figure 2 shows the printing subsystem, where $f_P(D)$ includes two steps of signal conversions as follows. First, *CIE-XYZ* tristimulus input T is transformed into CIE-RGB signal x_{RGB} by 3 × 3 linear matrix M_{RGB} as

$$x_{RGB} = [R, G, B]^t = M_{RGB} T \tag{3}$$

Next, x_{RGB} is converted into logarithmic density signal D_{RGB} as

$$D_{RGB} = [-\log_{10} R, -\log_{10} G, -\log_{10} B]^t = [D_R, D_G, D_B]^t \tag{4}$$

The matrices M_{SCAN} and M_{PRNT} are optimized to minimize the approximation errors in Eqs. 1 and 2 by the method of least squares.

Subspace Models

In the simple color matching system, single matrix M_{SCAN} in scanner and M_{PRNT} in printer are uniformly applied to

Original manuscript received March 24, 1998

* E-mail : ikaragoz@obs.gata.edu.tr

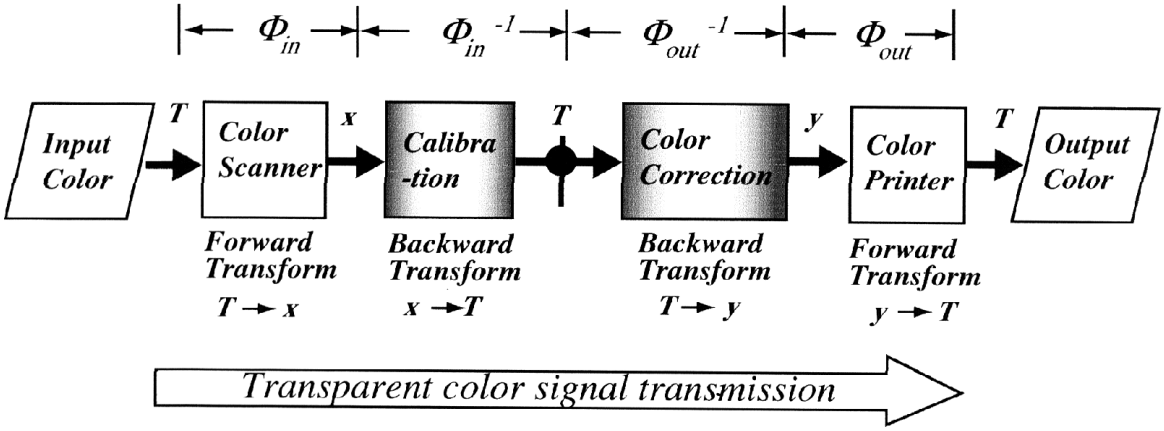

Figure 1. Basic color reproduction system model

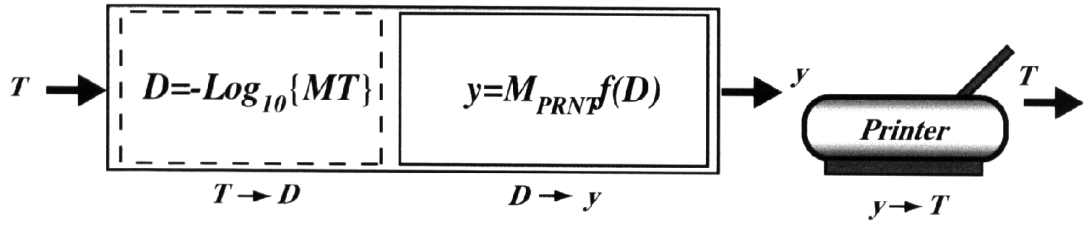

Figure 2. Printing sub-system model.

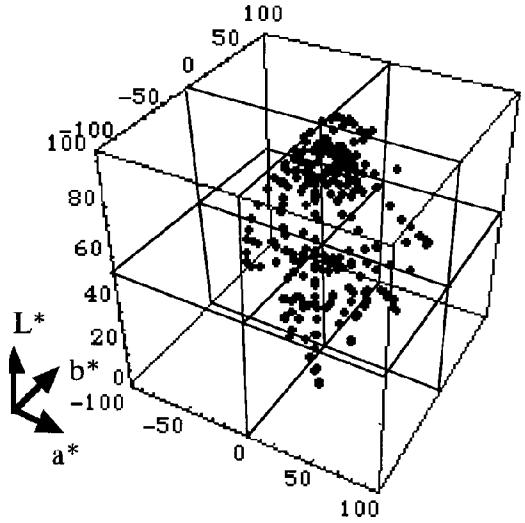

Figure 3. Uniform tri-linear division.

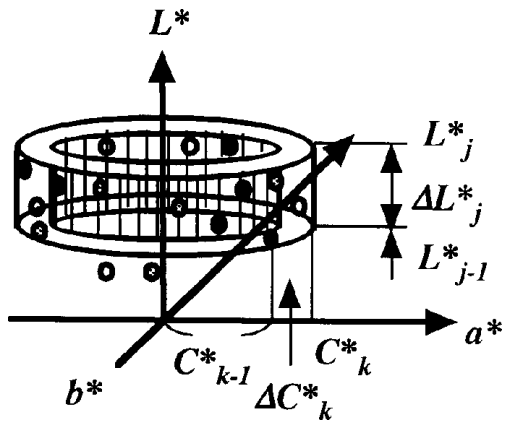

Figure 5. LC division.

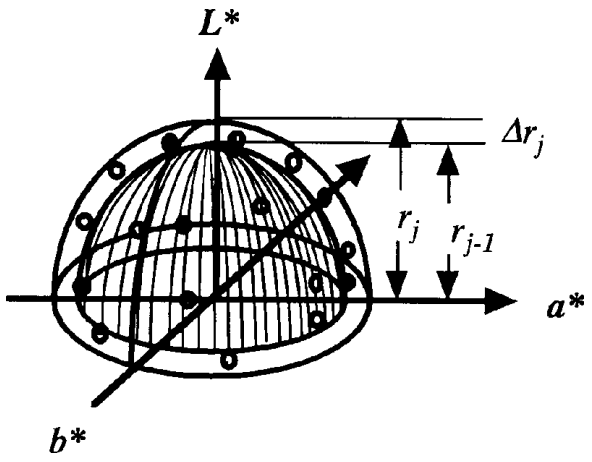

Figure 4. LAB vector division.

correct all of the pixels in the whole color space. On the contrary, here the color space is partitioned into a plurality of subspaces and different color matching matrices are applied to the subdivided color spaces. A simple way to do this is to divide each axis by an equal interval where the subspace is formed by tri-linear box with constant volume as shown in Fig. 3, where the printed sample color targets are not distributed uniformly inside the gamut of actual color printers. Then the equally divided subspaces include an uneven number of sample points in each subspace. The smaller the volume of subspace, the higher the color matching accuracy. However, as the number of partitions increases in the conventional tri-linear division, enough sample numbers to determine the color masking coefficients are not always guaranteed in every cube.

Figures 4, 5, and 6 illustrate the proposed partitioning methods into subspaces in CIELAB space. Here all the subspaces are partitioned to include the same num-

ber of color samples bounded with nonuniform intervals.

In Figure 4, CIELAB color space is partitioned into M subspaces divided by one dimensional LAB vector magnitudes.

1. LAB Vector Division; N divisions in LAB vector radius r

$$r_j \geq \Delta r_j > r_{j-1}; j = 1 \sim M \tag{5}$$

$$r = \{L^{*2} + a^{*2} + b^{*2}\}^{1/2} \tag{6}$$

Here the boundary radius r_j is determined to include the constant sample points in every subspace volumes.

Figure 5 illustrates the two-dimensional luminance-chrominance (LC) division, where CIELAB color space is partitioned into *totally* $M = J \times K$ subspaces along the following two directions.

2. LC Division; *J divisions in L^* and K divisions in C^**

$$L^*_j \geq \Delta L^*_j \geq L^*_{j-1}; \qquad j = 1 \sim J \tag{7}$$

$$C^*_k \geq \Delta C^*_k \geq C^*_{k-1}; \qquad k = 1 \sim K \tag{8}$$

$$C^* = \{a^{*2} + b^{*2}\}^{1/2} \tag{9}$$

Here the boundary luminance L^*_j and chroma C^*_k are determined to include the constant sample points in every subspace areas divided by ΔL^*_j and ΔC^*_k.

Figure 6 illustrates the polar coodinates division, where CIELAB color space is partitioned into totally $M = J \times K$ subspaces along the following two directions.

3. Polar Division; *J divisions in hue angle and K divisions in LAB vector radius r*

$$\theta_j \geq \Delta\theta_j \geq \theta_{j-1}; \qquad j = 1 \sim J \tag{10}$$

$$\theta = \tan^{-1}(b^*/a^*) \tag{11}$$

$$r_k \geq \Delta r_k \geq r_{k-1}; \qquad k = 1 \sim K \tag{12}$$

Here the sector angle θ_j and radius r_k are determined to include the constant sample points in every subspace area surrounded by $\Delta\theta_j$ and θr_k.

Calibration for Scanner

In the calibration of the scanner, IT8/7.2 standard color targets are used as inputs. Here, the XYZ tristimulus values $T_n = [X_n, Y_n, Z_n]^t$ for $n = 1 \sim N$=256 color chips are measured by spectro-colorimeter as original test targets. Thus the sample number Q of color chips included in each subspace is set as

$$Q = N/M = \text{constant} \tag{13}$$

The boundaries between subspaces in the proposed three division methods are determined for each subspace to include Q sample chips.

Letting the color scanner RGB signals be x_q^m ($q = 1 \sim Q$, $m = 1 \sim M$) corresponding to the input XYZ tristimulus values T_q^m for the m-th subspace, the calibration is performed by the following mathematical transformation.

$$\hat{T}_q^m = M_S^m f_S(x_q^m) \cong T_q^m \tag{14}$$

Here the scanner signal x_q^m is transformed to be matched to T_q^m by a polynomial expansion $f_S(\arg)$ and the coefficient matrix M_{SCAN} is decomposed into $\{M_S^m\}$ for individual subspace $m = 1 \sim M$.

The matrix M_S^m is optimized so as to minimize the mean square error between the original tristimulus value T_q^m and the approximation $\hat{T}_q^m$

$$e^2 = \frac{1}{Q}\sum_{q=1}^{Q}\left\{\left\|T_q^m - \hat{T}_q^m\right\|^2\right\} = \frac{1}{Q}\sum_{q=1}^{Q}\left\{\left\|T_q^m - M_S^m f_S(x_q^m)\right\|^2\right\} \tag{15}$$

Therefore the solution is given by

$$M_S^m = \left[T_Q^m f_S^t(x_Q^m)\right]\left[f_S(x_Q^m) f_S^t(x_Q^m)\right]^{-1} \tag{16}$$

where, T_q^m denotes the tristimulus matrix of Q samples in m-th subspace.

$$T_Q^m = \begin{bmatrix} X_1^m, & X_2^m, & \ldots, & X_Q^m \\ Y_1^m, & Y_2^m, & \ldots, & Y_Q^m \\ Z_1^m, & Z_2^m, & \ldots, & Z_Q^m \end{bmatrix} \tag{17}$$

Also, x_q^m denotes the scanner signal matrix of Q samples in m-th subspace.

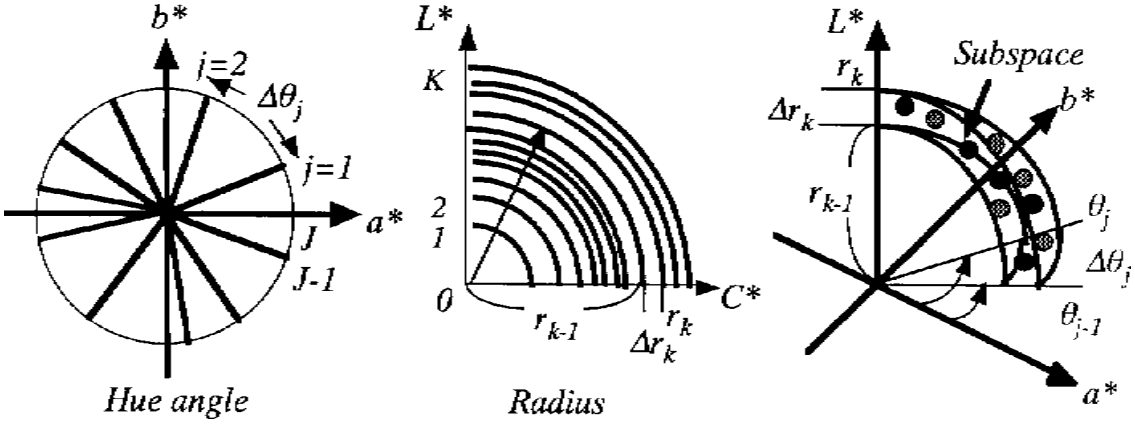

Figure 6. Polar coordinate division

$$x_q^m = \begin{bmatrix} R_1^m, & R_2^m, & \ldots, & R_Q^m \\ G_1^m, & G_2^m, & \ldots, & G_Q^m \\ B_1^m, & B_2^m, & \ldots, & B_Q^m \end{bmatrix} \tag{18}$$

and $f_S(x_q^m)$ represents the scanner signal matrix expanded by polynomials of Q samples in the same m-th subspace. For example, in the case of second order polynomials, it is given by 10 terms x Q samples matrix as follows.

$$f_S(x_Q^m) = \begin{bmatrix} R_1^m, & R_2^m, & \ldots, & R_Q^m \\ G_1^m, & G_2^m, & \ldots, & G_Q^m \\ B_1^m, & B_2^m, & \ldots, & B_Q^m \\ (R_1^m)^2, & (R_2^m)^2, & \ldots, & (R_Q^m)^2 \\ (G_1^m)^2, & (G_2^m)^2, & \ldots, & (G_Q^m)^2 \\ (B_1^m)^2, & (B_2^m)^2, & \ldots, & (B_Q^m)^2 \\ (R_1^m G_1^m), & (R_2^m G_2^m), & \ldots, & (R_Q^m G_Q^m), \\ (G_1^m B_1^m), & (G_2^m B_2^m), & \ldots, & (G_Q^m B_Q^m), \\ (B_1^m R_1^m), & (B_2^m R_2^m), & \ldots, & (B_Q^m R_Q^m), \\ 1, & 1, & \ldots, & 1 \end{bmatrix} \tag{19}$$

Color Correction for Printer

Generally, the inverse transform $\Phi_{OUT}^{-1}(T)$ in a printer is processed as "color masking" to remove the crosstalk caused by unwanted absorption of colorants. In the model proposed here, it is also described in each subspace as well as in scanner calibration. The forward transfer function of the printer is characterized by measuring the tristimulus values $T_q^m = [X_q^m, Y_q^m, Z_q^m]^t$ of printed color patches for drive signal $y_q^m = [C_q^m, M_q^m, Y_q^m]^t$ as

$$T_q^m = \Phi_P^m(y_q^m) \tag{20}$$

Here, the N = 512 color patches are printed and their tristimulus values $T_n = [X_n, Y_n, Z_n]^t$; $n = 1 \sim N$ are measured by spectrocolorimeter. Then $\{T_n\}$ are partitioned into M sets of $\{T_q^m\}$, each including $Q = N/M$ samples for $q = 1 \sim Q$ in $m = 1 \sim M$ subspaces. The sample number of color chips in all the subspaces are set as constant Q. First, the measured tristimulus value T_q^m is converted into logarithmic density signal D_q^m corresponding to the *CMY* drive signal as given in Eqs. 3 and 4. Then, the inverse transform from T_q^m to y_q^m is approximated by polynomial expansion

$$\hat{y}_q^m = \Phi_P^{m-1}(T_q^m) = M_P^m f_P(D_q^m) \cong y_q^m \tag{21}$$

The coefficient matrix M_q^m is optimized to minimize the mean square error between the drive signal y_q^m and its approximation $\hat{y}_q^m$, that is given by

$$M_P^m = \left[y_Q^m f_P^t(D_Q^m)\right]\left[f_P(D_Q^m) f_P^t(D_Q^m)\right]^{-1} \tag{22}$$

$$D_Q^m = \begin{bmatrix} D_{R1}^m, & D_{R2}^m, & \ldots, & D_{RQ}^m \\ D_{G1}^m, & D_{G2}^m, & \ldots, & D_{GQ}^m \\ D_{B1}^m, & D_{B2}^m, & \ldots, & D_{BQ}^m \end{bmatrix} \tag{23}$$

$$f_P(D_Q^m) = \begin{bmatrix} D_{R1}^m, & D_{R2}^m, & \ldots, & D_{RQ}^m \\ D_{G1}^m, & D_{G2}^m, & \ldots, & D_{GQ}^m \\ D_{B1}^m, & D_{B2}^m, & \ldots, & D_{BQ}^m \\ (D_{R1}^m)^2, & (D_{R2}^m)^2, & \ldots, & (D_{RQ}^m)^2 \\ (D_{G1}^m)^2, & (D_{G2}^m)^2, & \ldots, & (D_{GQ}^m)^2 \\ (D_{B1}^m)^2, & (D_{B2}^m)^2, & \ldots, & (D_{BQ}^m)^2 \\ (D_{R1}^m D_{G1}^m), & (D_{R2}^m D_{G2}^m), & \ldots, & (D_{RQ}^m D_{GQ}^m), \\ (D_{G1}^m D_{B1}^m), & (D_{G2}^m D_{B2}^m), & \ldots, & (D_{GQ}^m D_{BQ}^m), \\ (D_{B1}^m D_{R1}^m), & (D_{B2}^m D_{R2}^m), & \ldots, & (D_{BQ}^m D_{RQ}^m), \\ 1, & 1, & \ldots, & 1 \end{bmatrix} \tag{24}$$

Experiments

These subspace models have been applied to a flat bed color scanner and color inkjet printer. In the experiments, N = 256 basic color chips in IT8/7.2 standard color targets were used for scanner calibration, while $N = 8^3 = 512$ color patch samples were generated on the inkjet printer driven by the 8 steps of cmy signals $y_i = [C_i, M_i, Y_i]^t$, and their tristimulus values $T_o = [X_o, Y_o, Z_o]^t$ were measured by spectro-colorimeter. For example, the color masking matrices in the printer are calculated by using these data set $\{y_i, T_o\}_{i,o=1 \sim 512}$.

In the uniform tri-linear division, CIELAB space is divided into tri-linear boxes with the same volume, where the number of color samples included in each subspace becomes uneven. In order to apply the higher order polynomials with P terms, each subspace should include at least $Q \geq P$ samples. Thus, for example, the whole color space was segmented into $M \leq 8$ cubes bounded at $a^* = 0$, $b^* = 0$, and $L^* = 50$, unless the sufficient samples could not be guaranteed for applying third order matrix (P = 20).

While in the LAB vector division, CIELAB space is segmented into M = 2~64 radial segments by $\{\Delta r_j\}_{j=1\sim63}$, including an equal number of samples in each. Also in LC division, the distributions of color sample values $LAB_i = [L^*_i, a^*_i, b^*_i]^t$ are first divided into J segments in L^* direction, each including N/J samples and next, the samples in each interval ΔL^*_j are again divided into K segments in C^* direction. Thus, whole color sample space is divided into totally $M = J \times K$ = 4~64 subspaces, each including N/M samples equally.

In the polar coodinates division, whole color sample space is first segmented into J hue angle sectors and next, the samples in each hue angle sector are again divided into K radial segments as well. In all subspace models, M has different coefficient matrices; M_S^m in the scanner or M_P^m in the printer for $m = 1 \sim M$ can be determined individually.

Results in Scanner Calibration. The calibration results for a flat bed scanner are given in Figs. 7 and 8 in comparison with conventional methods. Figure 7 shows root mean square (rms) color differences ΔE_{ab}*(rms) and Fig. 8 compares the maximum ΔE_{ab}*(max) both in the case of M = 8 division. In all cases, the calibration accuracy has been improved for the higher order polynomials. Although the third order polynomial resulted in ΔE_{ab}*(rms)≈1.0 without division, it was impossible for the case of uniform trilinear division to apply the third order matrix with M = 8 division because of insufficient sample numbers in some subspaces, and, moreover, the second order matrix did not give any credit to the linear matrix. This may be caused

by the uneven sample numbers between the subspaces. On the other hand, proposed division methods made it possible to apply the higher order terms and resulted in the dramatic improvements in calibration errors. The rms errors by the second order matrix method with M = 8, were ΔE_{ab}*(rms) = 0.90, 0.75, and 0.77 for *LAB* vector division, LC division, and polar division respectively. These errors have been further improved to ΔE_{ab}*(rms) = 0.47, 0.35, and 0.39 for the use of third-order terms. In addition to the rms errors, the maximum errors also tended to be dramatically improved by the proposed subspace division methods especially for the use of higher-order polynomials as shown in Fig. 8. The maximum calibration errors were ΔE_{ab}*(max) = 5.9, 4.3, and 4.9 by second-order, and ΔE_{ab}*(max) = 2.0, 1.58, and 2.0 by third-order polynomials for *LAB* vector division, LC division, and polar division respectively. Figure 9 illustrates how the calibration error decreases as the division number M increases. The rms errors are shown to be roughly reduced linearly with the division number M approaching zero. Theoretically, the calibration errors are expected to reach zero at the maximum division number $M = N/P$, where each sub-space includes the minimum sample number $Q = P$ just adequate to determine the P terms of the coefficient matrices $\{M_S^m\}$.

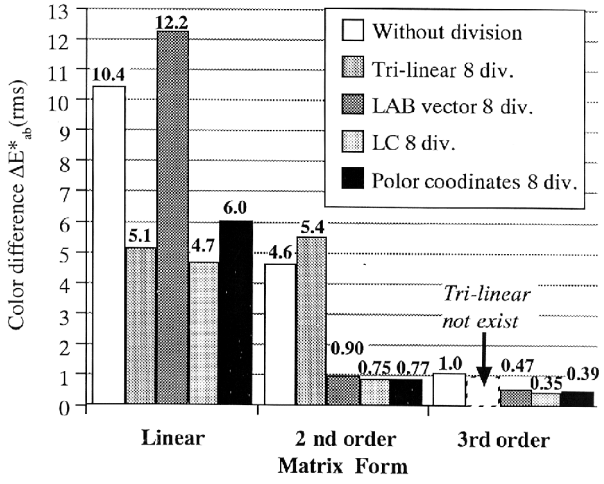

Figure 7. RMS error in scanner calibration (M = 8 division)

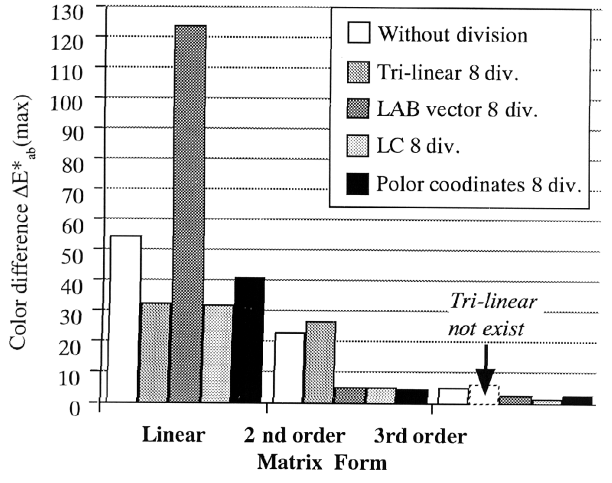

Figure 8. Maximum error in scanner calibration (M = 8 division)

Figure 10 shows the distributions of IT8/7.2 color targets in a^*-b^* plane after calibration. The proposed subspace division methods of LC division and polar coordinate division are shown to give highly accurate calibrations almost close to original targets as compared with conventional methods.

Results in Color Correction for an Inkjet Printer. Here the color correction experiments have been evaluated inside the printer color gamut, where the correction matrices are optimized using the printed color patches as input targets. The typical color correction results for the inkjet printer tested are summarized in Fig. 11 (a) and (b) compared with conventional methods for the case of M = 8 division. Figure 11(a) shows rms color differences; ΔE_{ab}* (rms) for trained color targets where N = 512 color patches are generated by a combination of CMY printer drive signals and measured *XYZ* values are used to determine the coefficient matrices $\{M_P^m\}$. In Fig. 11(b), N = 512 non-trained color targets are also used for the estimation; these are generated by a different combination of *CMY*s. In our experiments, the color corrections worked very well for non-trained targets as well as trained targets with almost the same accuracy.

As clearly shown, the subspace division methods resulted in higher precision color matching than the conventional single matrix method without division. In general, it is possible to extremely reduced the color differences by nonlinear color correction using higher order polynomials. However, in the uniform tri-linear division, the best result was given by second-order correction, while rms color difference increased for third-order correction. This may be caused by the unbalanced color sample numbers in uniformly divided subspaces. The best correction for trained targets was obtained by LAB vector division with third-order polynomials, resulting in ΔE_{ab}*(rms)≈1.5. In the correction for non-trained targets, the best result was obtained by LC division with third-order polynomials, resulting in ΔE_{ab}*(rms) ≈ 2.1.

Polar coordinate division showed stable and excellent results in both trained and non-trained estimations. It resulted in ΔE_{ab}*(rms) ≈ 2.7 by second-order and ≈ 2.2

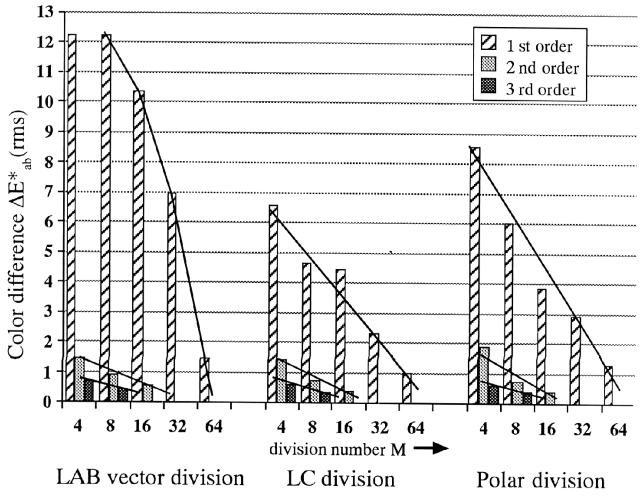

Figure 9. Charge in RMS error versus number of division in scanner calibration.

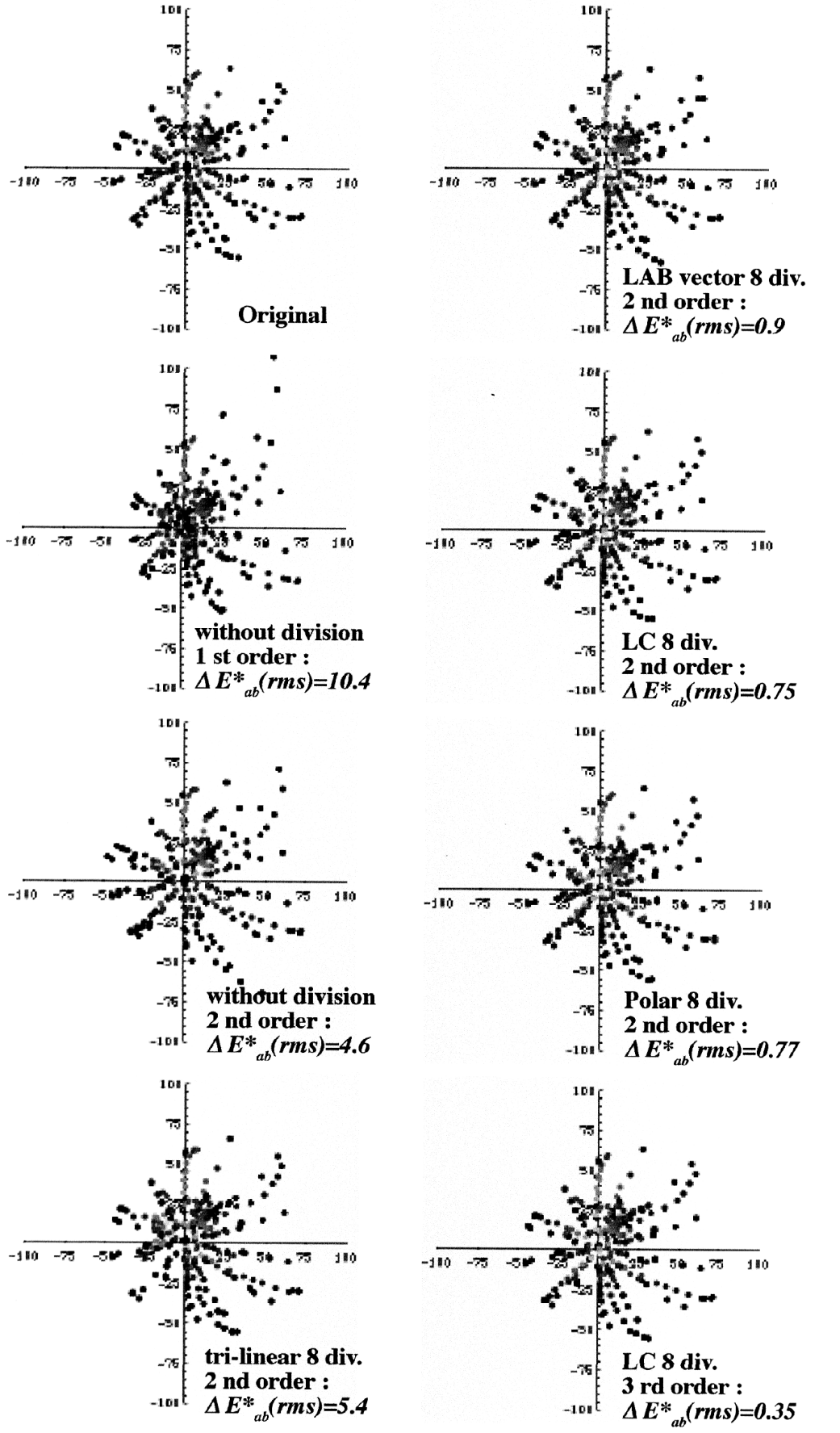

Figure 10. Color distributions after scanner calibration in a*-b*

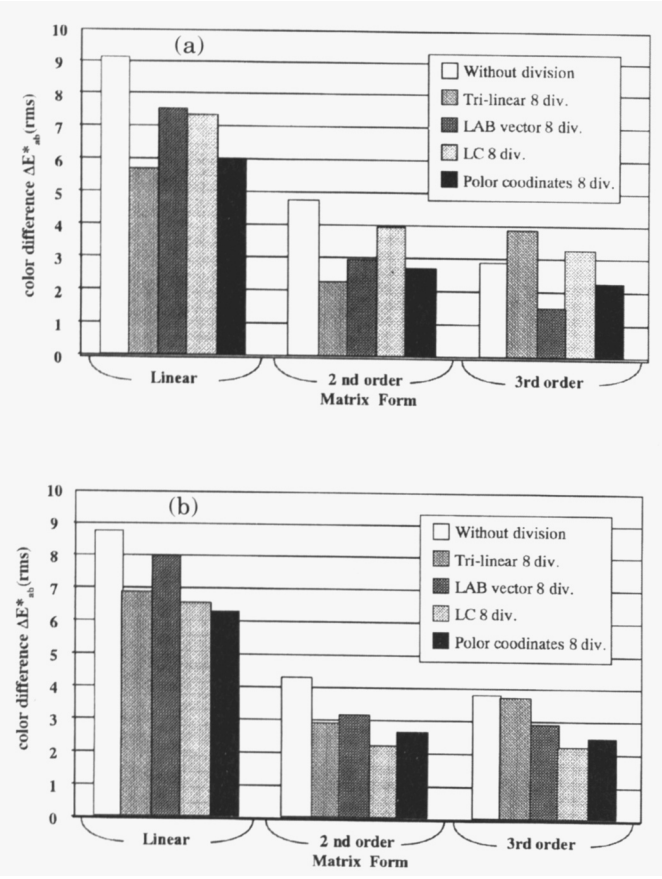

Figure 11. RMS error in printer correction. (a) Trained targets (M = 8 division); (b) non-trained targets (M = 8 division).

by third-order correction for trained targets and ΔE_{ab}*(rms) ≈ 2.6 by second-order and ≈ 2.4 by third-order correction for non-trained target. The maximum error ΔE_{ab}*(max) in the printer also showed similar behavior as well as the rms color differences.

Figure 12 illustrates how the correction error decreases as the division number M increases in the case of trained targets. The rms errors are reduced almost monotonously with the division number M. *LAB* vector division gives excellent accuracy in spite of one-dimensional division. The optimum color differences in Polar coordinate division as well as *LAB* vector division approach around ΔE_{ab}*(rms) ≈ 1.5 as the division number M increases. However, the third-order correction errors in LC division slightly increased with M. These errors may be enhanced by small mismatches in the higher-order coefficient terms.

Figure 13 shows the distributions of reproduced color targets in a*-b* plane after printer correction. As clearly shown, the subspace division methods offer higher precision color matching than the conventional single matrix method.

Discussion and Conclusion

The high precision color calibrations for input/output devices have been approached by optimization in subdivided color spaces. Nonuniform division to subspaces, including equal numbers of color samples in each, makes it possible to use the higher order nonlinear matrices. In the application to a scanner, the calibration accuracy could be dra-

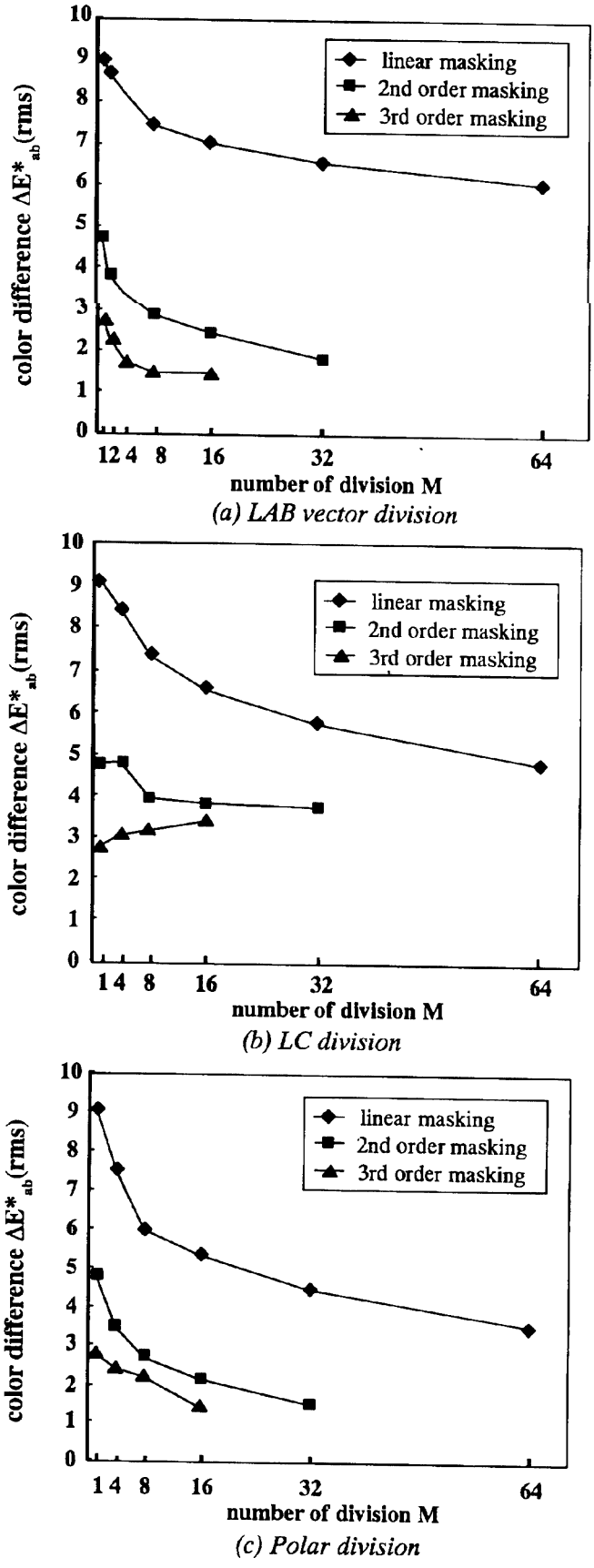

Figure 12. Change in rms error versus number of division in printer correction (trained targets).

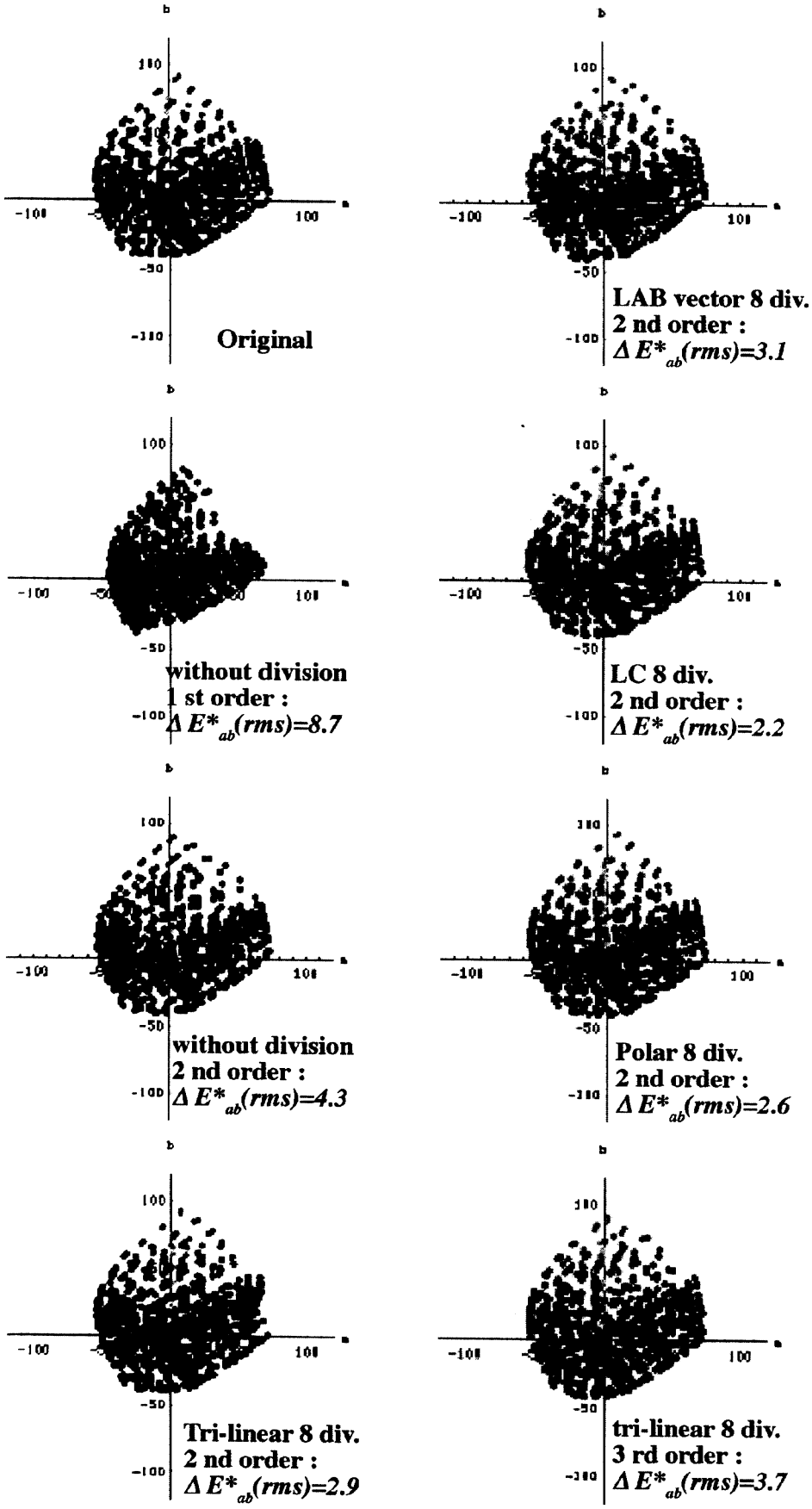

Figure 13. Color distributions after printer correction in a*-b* plane.

matically improved by operating the nonlinear matrices with second-order or third-order polynomials optimized in each subspace. The rms color differences as well as maximum color differences could be reduced to about one-fifth or less as compared with conventional methods, reaching to ΔE_{ab}*(rms) ≈ 0.35 and ΔE_{ab}*(max) ≈ 1.6. These values are considered to be equal to the limits in colorimetric measurement stabilities.

In the application to printer color correction, the proposed subspace division method resulted in high precision reproductions with ΔE_{ab}*(rms) ≈ 2~3 for inkjet printers in low-end consumer use. As compared with conventional color transforms by single matrix, the color errors in the proposed methods could be reduced to two-thirds or less inside the device gamuts. One-dimensional *LAB* vector division worked well for higher order polynomials. Two-dimensional polar coordinate division was stable for both trained and non-trained targets. Because each subspace surrounded by $\Delta\theta_j$ in hue angle and Δr_k in radial direction will include the color samples and resemble in hue and colorfulness, the coefficient matrix is expected to fit well in the statistical variances. *LAB* vector 8 division with third-order matrix resulted in the highest reproduction with ΔE_{ab}*(rms) ≈ 1.5 and polar coordinate 16 division with third-order matrix also approached to ΔE_{ab}*(rms) ≈ 1.5 for trained targets. LC division with third-order matrix resulted in the highest quality reproduction with ΔE_{ab}*(rms) ≈ 2.1 for non-trained targets. These values almost approach mechanical stability around ΔE_{ab}*(rms) ≈ 1.0, in low-end inkjet printers.

The gamut compression process is not included in this article but is necessary for the inputs outside the printer gamut and is under development.

References

1. H. Kotera, Color Rendition in Digital Printing, *JIIEEJ*, **14,** 5, 298–307 (1985).
2. H. Ikegami, New direct color mapping method for reducing the storage capacity of look-up table memory, *Proc. SPIE* **1075,** pp. 26–31 (1989).
3. P. C. Hung, Colorimetric Calibration for scanners and media. *Proc. SPIE* **1448,** 164–174 (1991).
4. K. Kanamori and H. Kotera, Color correction Technique for Hard Copies by 4-Neighbors Interpolation Method, *J. Imaging Sci. Technol.* **36,** 1, 73–80 (1992).
5. R. Balasubramainen, Color Transformations for Printer Color Correction, *Proc. 2nd Color Imaging Conf.*, IS&T, Springfield, VA, 1994, pp. 62–65.
6. H. Haneishi, T. Hirao, A. Shimazu, and Y. Miyake, Colorimetric Precision in Scanner Calibration Using Matrices, *Proc. 3rd Color Imaging Conf.*, IS&T, Springfield, VA, 1995, pp. 106–108.
7. T. Johnson, Methods for characterizing colour scanners and digital cameras, *Displays*, **16,** 183–192 (1996).
8. T. Johnson, Methods for characterizing colour printers, *Displays* **16,** 4, 193–202 (1996).
9. A. Ishige, C. Hung-Shing and H. Kotera, High Presision Device Calibration in Sub-divided Color Spaces, *Proc. PPIC/JH'98P58*, 375–378 (1998).